SANDIA REPORT

SAND2010-3828
Unlimited Release
Printed June 2010

Doppler Characteristics of Sea Clutter

Ann Marie Raynal, Armin W. Doerry

Prepared by
Sandia National Laboratories
Albuquerque, New Mexico 87185 and Livermore, California 94550

Sandia National Laboratories is a multi-program laboratory operated by Sandia Corporation,
a wholly owned subsidiary of Lockheed Martin Corporation, for the United States Department of Energy's
National Nuclear Security Administration under Contract DE-AC04-94AL85000.

Approved for public release; further dissemination unlimited.

Sandia National Laboratories

Issued by Sandia National Laboratories, operated for the United States Department of Energy by Sandia Corporation.

NOTICE: This report was prepared as an account of work sponsored by an agency of the United States Government. Neither the United States Government, nor any agency thereof, nor any of their employees, nor any of their contractors, subcontractors, or their employees, make any warranty, express or implied, or assume any legal liability or responsibility for the accuracy, completeness, or usefulness of any information, apparatus, product, or process disclosed, or represent that its use would not infringe privately owned rights. Reference herein to any specific commercial product, process, or service by trade name, trademark, manufacturer, or otherwise, does not necessarily constitute or imply its endorsement, recommendation, or favoring by the United States Government, any agency thereof, or any of their contractors or subcontractors. The views and opinions expressed herein do not necessarily state or reflect those of the United States Government, any agency thereof, or any of their contractors.

Printed in the United States of America. This report has been reproduced directly from the best available copy.

Available to DOE and DOE contractors from
U.S. Department of Energy
Office of Scientific and Technical Information
P.O. Box 62
Oak Ridge, TN 37831

Telephone:	(865) 576-8401
Facsimile:	(865) 576-5728
E-Mail:	reports@adonis.osti.gov
Online ordering:	http://www.osti.gov/bridge

Available to the public from
U.S. Department of Commerce
National Technical Information Service
5285 Port Royal Rd.
Springfield, VA 22161

Telephone:	(800) 553-6847
Facsimile:	(703) 605-6900
E-Mail:	orders@ntis.fedworld.gov
Online order:	http://www.ntis.gov/help/ordermethods.asp?loc=7-4-0#online

SAND2010-3828
Unlimited Release
Printed June 2010

Doppler Characteristics of Sea Clutter

Ann Marie Raynal
Radar and Signal Analysis Department
Armin W. Doerry
SAR Applications Department
Sandia National Laboratories
P.O. Box 5800
Albuquerque, New Mexico 87185-MS0519

Abstract

Doppler radars can distinguish targets from clutter if the target's velocity along the radar line of sight is beyond that of the clutter. Some targets of interest may have a Doppler shift similar to that of clutter. The nature of sea clutter is different in the clutter and exo-clutter regions. This behavior requires special consideration regarding where a radar can expect to find sea-clutter returns in Doppler space and what detection algorithms are most appropriate to help mitigate false alarms and increase probability of detection of a target. This paper studies the existing state-of-the-art in the understanding of Doppler characteristics of sea clutter and scattering from the ocean to better understand the design and performance choices of a radar in differentiating targets from clutter under prevailing sea conditions.

ACKNOWLEDGMENTS

This report was funded by General Atomics Aeronautical Systems, Inc. (ASI) Reconnaissance Systems Group (RSG). The authors would also like to thank Doug Bickel and Ruby Pai for providing guidance regarding the existing literature of sea clutter.

CONTENTS

FIGURES

TABLES

NOMENCLATURE

dB	Decibels
DOE	Department of Energy
cm	Centimeters
GHz	Gigahertz
HF	Radar frequencies between 3-30 megahertz
HH	Horizontal polarization
Hz	Hertz
kHz	Kilohertz
L-band	Radar frequencies between 1-2 gigahertz
LFM	Linear, frequency-modulated
MHz	Megahertz
m	Meters
ms	Milliseconds
PRF	Pulse repetition frequency
RCS	Radar cross section
SNL	Sandia National Laboratories
VHF	Radar frequencies between 30-300 megahertz
VV	Vertical polarization
X-band	Radar frequencies between 8-12 gigahertz

Katsushika Hokusai's *The Great Wave off Kanagawa*, Color on Wood, Japan circa 1829–32

1. INTRODUCTION

Doppler radars can distinguish targets from clutter if the target's velocity along the radar line of sight is beyond that of the clutter. Some targets of interest may have a Doppler shift similar to that of clutter. Usually the radar backscatter from the open ocean, or sea clutter, is low enough that these targets can be detected. However, the nature of the return is different in the clutter and exo-clutter regions. For optimal radar performance, different detection algorithms should be used in the two regions. Therefore, an understanding of where the boundary lies between exo-clutter and endo-clutter regions of Doppler space, and where in Doppler space we can expect to find sea-clutter returns, is important for determining the detection algorithms to apply to each region. Furthermore, an understanding of the scattering nature of the ocean can help mitigate false alarms. Lastly, if a radar has Doppler processing problems, understanding the influence of the ocean's Doppler spectrum to the overall Doppler space allows phenomenology to be discarded as a potential radar issue. In consideration of all these factors, the motivation for studying the Doppler characteristics of sea clutter is to better understand the design and performance choices of a radar in differentiating targets from clutter under prevailing sea conditions.

Determining the Doppler characteristics of sea clutter is fundamentally an electromagnetic scattering and mathematical modeling problem, though empirical observations of scattering behavior and characteristics dominate the literature. The Doppler characteristics of sea clutter depend on many parameters of a radar and the ocean which impact scattering phenomenology including polarization, frequency, look angle of the radar relative to wind direction, grazing angle, sea state, wave velocities, and the types of ocean waves present [1]. The sea clutter Doppler spectrum is the Fourier transform along slow time for a range cell of an image of the sea, usually represented as a power spectra [2]. More formally, for a band-limited complex time signal

$$Z(t) = E_I(t) + jE_Q(t)$$

between $-\frac{T}{2} < t < \frac{T}{2}$ and 0 otherwise, where E represents the in-phase (I) and quadrature (Q) channel voltages, the Doppler power spectrum will be:

$$S(\omega) = \frac{|Z(\omega)|^2}{2\pi T}$$

where $Z(\omega)$ is the Fourier transform of the complex signal ($Z(\omega) = \int_{-\infty}^{\infty} e^{j\omega t} Z(t)dt$). Modeling of the Doppler spectrum characteristics is dependent on the signal integration time interval, T, and properties of the wave phenomenon, which are discussed in more detail in subsequent sections.

This document is organized as follows. Section 2 covers the types of waves that form the principal backscattering mechanisms of the ocean at radio frequencies. Section 3 details empirical observations regarding ocean backscatter and how it relates to the Doppler spectrum of sea clutter. Section 4 explains specific mathematical models that exist for analytically describing the shape and shift of the measured Doppler spectra of sea clutter. Section 5 describes electromagnetic modeling related to sea scattering and clutter. Lastly, Section 6 provides a concluding summary.

Roll on, thou deep and dark blue Ocean--roll!
Ten thousand fleets sweep over thee in vain;
Man marks the earth with ruin--his control
Stops with the shore.

- Lord Byron

2. OCEAN WAVE CHARACTERISTICS

Ocean wave behavior can appear incredibly complex, but fundamentally all ocean waves are sinusoids of different wavelengths and amplitudes that interact to form more complex structures. Many sources, such as currents, weather, surface tension, and gravity contribute to the wide variety of wave structures in the ocean. At radio frequencies, backscatter from the open ocean is predominantly from surface waves caused by wind and the degree of roughness of this surface, known as sea state. These surface waves can be resonant or non-resonant. The two types of resonant surface wave phenomena that appear in the literature when it comes to the Doppler spectrum of sea clutter are capillary and gravity waves [1]. They are categorized by the restoring forces that act on them. Breaking waves are the main type of non-resonant phenomena of the ocean surface that is of interest to the radar community. The nature and interactions of all these waves form an important basis for understanding microwave scattering from the ocean surface, and hence the Doppler characteristics of sea clutter.

2.1. Resonant Waves

1.1.1. Capillary Waves

Capillary waves, also known as ripples, are small waves less than 1.73 cm in wavelength. Capillary waves are caused by wind blowing over the surface of the water. Their phase velocity is determined primarily by the restoring force from the surface tension of the water. These waves ride atop of, and are modulated by, longer waves known as gravity waves. Capillary waves essentially form the microstructure of the resonant waves on the ocean surface.

1.1.1. Gravity Waves

Gravity waves are long-wavelength waves, which are greater than 1.73 cm in wavelength up to a few hundred meters. Their propagation velocity is determined primarily by the restoring force of gravity, which is typically referred to as the wave or group velocity of propagation of the wavefronts. A second velocity, known as the orbital velocity, describes movement of water that is not propagating, but rather, is a localized rotating particle velocity of the wave.

Gravity waves are also caused by wind, and form the macrostructure of resonant waves on the ocean surface [2]. They are subdivided into two categories: sea and swell. Gravity waves from the blowing of a local wind are called sea. If a local wind has blown for a sufficient time and distance (known as duration and fetch) in a given direction, the wave structure reaches an equilibrium state called a fully developed sea. Once sea waves propagates away from the local wind, then they are called swell. Swell is therefore, extremely long-wavelength, low-amplitude, nearly perfect sinusoidal waves that arrive somewhere from a distant, non-local, wind and that can exist without local wind.

2.2. Non-Resonant Waves

Breaking waves are non-resonant effects that detach from the resonant wave surface. A wave breaks by first increasing in height such that it sharpens at the top and flattens at the bottom, until the sharp crest becomes so steep that it curls and rolls down the front of the wave slope surface. In microwave scattering, the sharpening and flattening stage of a breaking wave is called a burst; the curling and rolling stage is known as a whitecap. Breaking can happen when the vertical acceleration of the surface reaches a threshold related to the acceleration of gravity, the wave crest velocity exceeds the orbital velocity of a wave, and the pressure at the free surface exceeds the limits of Bernoulli equations for hydrodynamics. Based on the analysis of a particular kind of surface wave known as a Stokes wave, the following four rules of thumb apply for a wave to break. First, the wave steepness, or ratio of the vertical peak-to-trough height to the horizontal peak-to-peak wavelength, must exceed 0.142. Second, the vertical acceleration of the wave must exceed $\frac{-g}{2}$, where g is the acceleration due to gravity. Third, the surface slope must exceed $\tan\left(\frac{\pi}{6}\right)$ or about 0.58. Fourth, the fluid velocity to phase speed ratio of the wave must exceed 0.47. Surface slope, wave steepness, and vertical acceleration are related such that one of those parameters along with fluid velocity to phase speed ratio are sufficient to determine if a wave will break.

2.3. Sea State

Sea state is the qualitative and quantitative roughness of the sea surface. Specifically, sea state is quantified by a term known as significant wave height, or the average height of the highest one-third of the waves in a wave train. A qualitative human description for the sea is then associated with this value and other sea parameters. There are many scales for sea state: the Douglas scale, the Hydrographic Office scale, the World Meteorological Organization (WMO) scale, and the Beaufort scale (which actually measures wind speed). An approximate combination of the Douglas, Beaufort, and WMO scales are provided for reference in Table 1. Figure 1 includes images of the sea for the Beaufort scale for reference as well. The average sea state for the world's oceans typically occurs at a wind speed of 15 knots and significant wave height of approximately 2.5 m. Note that 1 knot is approximately 0.5144 m/s.

Table 1. Sea State Characteristics from Ref. [2, 3]

WMO / Douglas Sea State	WMO Significant Wave Height (m)	Douglas Wind Speed (knots)	Douglas Duration/ Fetch (hours/nautical mile)	WMO Sea State Category	Approximate Beaufort Wind and Sea Description
0	0	-	-	Calm (glassy)	Calm wind; Sea like a mirror
1	0-0.1	-	-	Calm (rippled)	Light air; Sea has scaly ripples
2 / 1	0.1-0.5	<6	1/20	Smooth (wavelets)	Light breeze; Sea has small, short wavelets; glassy crests
3 / 2	0.5-1.25	6-12	5/50	Slight	Gentle breeze; Sea has large wavelets; breaking crests; glassy foam; scattered whitecaps
4 / 3	1.25-2.5	12-15	20/120	Moderate	Moderate breeze; Sea has small waves; frequent whitecaps
5 / 4	2.5-4	15-20	23/150	Rough	Fresh breeze; Sea has moderate, longer waves; many whitecaps
6 / 5	4-6	20-25	25/200	Very rough	Strong breeze; Sea has large waves; extensive whitecaps
7 / 6	6-9	25-30	27/300	High	Near gale; Sea heaps up; white foam blown in streaks along wind direction
8 / 7	9-14	30-50	30/500	Very high	Gale to Storm; Moderately high to very high waves; white foam streaks along wind direction; violent toppling and rolling of crests
9 / 8	>14	>50	35/700	Phenomenal	Violent Storm to Hurricane; Exceptionally high waves; small to medium ships lost behind waves; white foam patches and spray everywhere

Figure 1. Images of the Beaufort Scale from Ref. [3]

3. Empirical Observations of the Doppler Spectrum

Much of the existing body of literature regarding the Doppler spectrum of sea clutter involves observational experiments from radars atop cliffs looking at the sea, controlled wave tank experiments, or the occasional airborne remote sensor mission. The knowledge gleaned from these experiments provides an intuitive understanding of scattering from ocean waves and its relationship to the qualitative Doppler characteristics of the sea clutter spectrum.

3.1. Scattering Mechanism Types and Behavior

Scattering occurs from surfaces that are on the order of the radar wavelength. As such, scattering from the sea surface may occur (and be linearly combined) in three different ways, depending on the radar frequency. This is called the three-component model and consists of Bragg, burst, and whitecap scattering [2].

3.1.1. Bragg Scattering

At low frequencies (i.e. HF and VHF), Bragg scattering is the only mechanism present in radar backscatter and involves resonant scattering from surface waves [1]. Bragg scattering is originally a term used to describe x-ray diffraction from crystals, whereby the structure of the crystal can be divided into molecular planes, separated by a periodic distance, that coherently reinforce in their scattering (i.e. a diffraction grating). The x-ray wavelength must be an integer multiple of twice the molecular plane spacing and is dependent on the look angle. Likewise, waves under the right conditions backscatter in a periodic way such that the return from multiple waves over the sea surface in the radar line of sight coherently reinforce. Bragg scattering for sea clutter strongly occurs if the radar wavelength is twice that of the water wavelength, but further depends on the grazing angle as:

$$\lambda_{\text{radar}} = 2\lambda_{\text{water}} \cos(\psi).$$

The characterization of the Doppler spectrum from Bragg scattering is attributed to Douglas Crombie [4], who in 1955 observed the periodicity of sea wave returns at HF. He offered the explanation that short trains of sea waves traveling in the radial direction of the radar would exhibit a discrete Doppler shift for zero grazing angle of the form

$$f_{\text{Doppler}} = \sqrt{\frac{g}{\pi}\frac{n}{\lambda_{\text{radar}}}}$$

where g is acceleration due to gravity, when $\lambda_{\text{water}} = \frac{n\,\lambda_{\text{radar}}}{2}$ for a positive integer n. Large scattering would occur for odd n and lesser scattering for even n. He likened these wave crest trains to a diffraction grating, where n can be considered the order of the diffraction grating. At low radar frequencies such as HF, the radar backscatter comes only from gravity waves and the Doppler shift is independent of sea state.

At much higher radar frequencies (i.e. wavelength less than 4 cm), Crombie postulated that Bragg scattering would be due to the capillary waves riding atop gravity waves and that they would produce a continuous Doppler spectrum for large n. This wave phenomenon is now called a two-roughness or composite surface model [2] because Bragg scattering occurs at two scales, the capillary and gravity wavelengths. The peak Doppler shift for the composite surface model occurs at a frequency of

$$f_{\text{Doppler}} = \frac{2}{\lambda_{\text{radar}}}(v_B + v_D)\ .$$

Here, v_B is the Bragg resonant scattering wave velocity given by

$$v_B = \sqrt{\frac{g}{k_{\text{B}}} + \gamma k_{\text{B}}},$$

for a surface tension per bulk density, γ, and Bragg resonance wave number,

$$k_{\text{B}} = 2\ \frac{2\pi}{\lambda_{\text{radar}}}\ \cos(\psi).$$

Note that v_B is composed of two terms that describe the general motion of the waves. The first term is the phase velocity of the wave due to gravity; the second term is that due to surface tension. For long-wavelength, gravity waves, the first term dominates and we arrive at Crombie's Doppler frequency solution for HF. For short, capillary waves, surface tension dominates in determining the Bragg scattering Doppler characteristics at the higher microwave frequencies. As for v_D, it represents the drift and orbital velocities of the gravity waves which modulate the capillary waves as,

$$v_D = \left(\frac{H}{2}\right)^2 \left[\frac{\omega k \cosh(2kd)}{2\sinh^2(kd)}\right] \cos\theta,$$

where H is the height between a wave crest and trough, ω and k are the wave angular velocity and wave number, d is the water depth [5, 6], and θ is the wind direction [7]. For deep ocean with large water depth, the above would (in the limit) go to

$$v_D = \left(\frac{H}{2}\right)^2 \omega k \cos\theta,$$

since surface wave, and not wave current, effects are of concern.

The temporal and Doppler behavior of Bragg scattering can be seen in Figure 2 (as borrowed from the results of reference [5]) as a function of polarization and wind direction for an X-band radar. The center frequency of the radar was 9.75 GHz, with a 2 kHz PRF, 500 MHz LFM chirp, Doppler bandwidth of +/-500 Hz per polarization with pulse-to-pulse polarization. The radar was on a cliff 64 m above sea level with 3.6 degrees of grazing angle. Time profiles of both vertical and horizontal polarizations show that Bragg scattering for the vertical polarization (VV) is much stronger in amplitude than the horizontal (HH) direction. When the radar frequency is not low (i.e. HF or VHF) and the grazing angle is between 20 to 70 degrees, the magnitude of Bragg scattering is high compared to other mechanisms. This observation is not so at other grazing angles, however. The decorrelation time is on the order of tens of milliseconds for the scattering phenomenon, which lasts on the order of seconds. The sea clutter Doppler spectrum at high frequencies (usually L-band and higher) is broad and low near zero frequency shift. The Doppler shift and shape is about the same irrespective of polarization. The phenomenon is also consistent with wind direction relative to the radar line of sight. Reference [2] indicates that cross polarization amplitudes are small for Bragg scattering and that the magnitude is halved for circular polarization because of the vertical polarization dominance. These effects are shown in Figure 3 from reference [2] for an X-band radar.

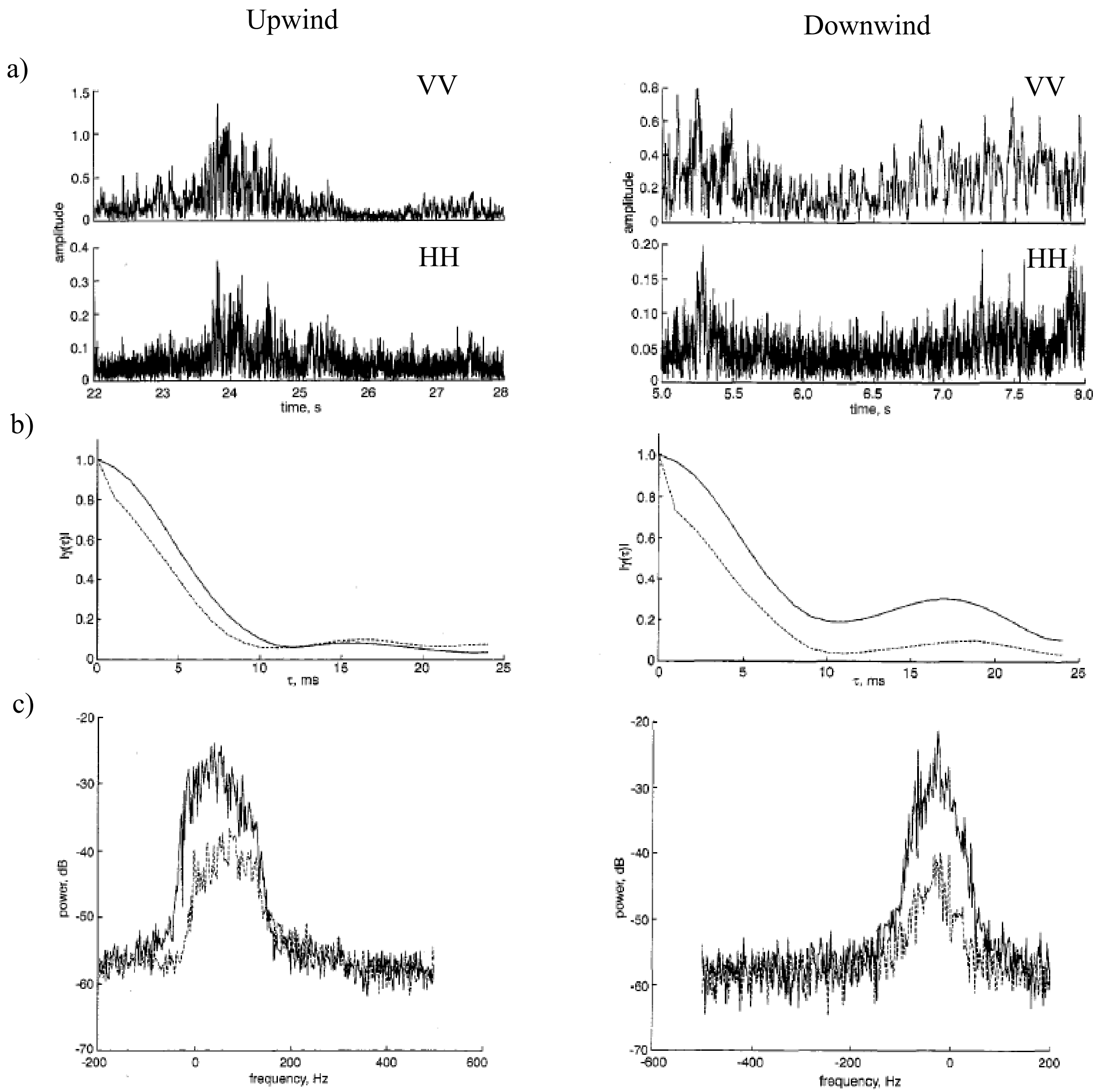

Figure 2. Bragg scattering behavior from Ref. [5]
a) Time profile, b) Autocorrelation, c) Doppler spectrum (VV = solid, HH = dotted, unless otherwise specified)

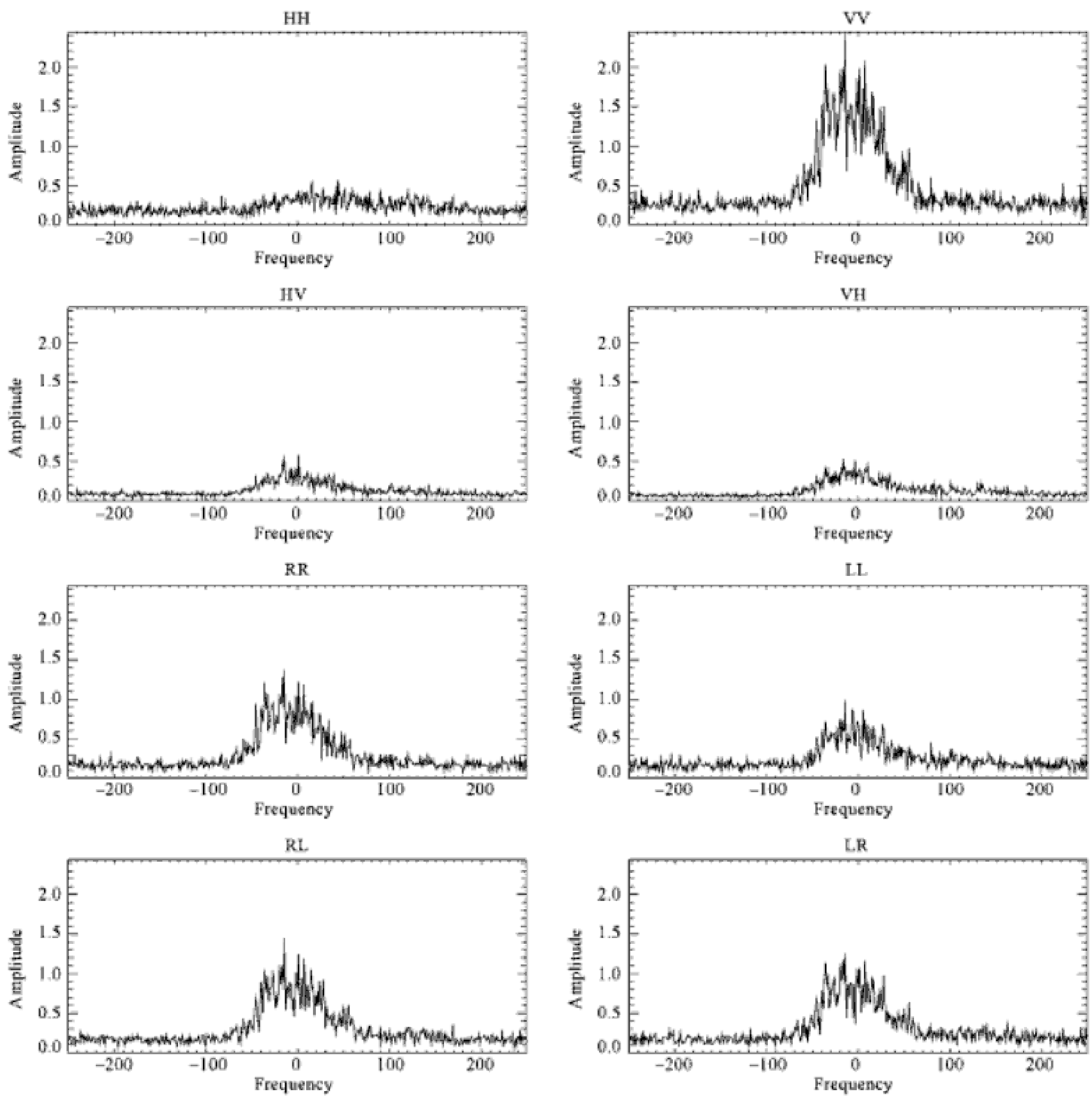

Figure 3. Bragg scattering cross-polarization and circular polarization Doppler spectrums at X-band from Ref. [2]

3.1.2. Burst Scattering

Burst scattering, also known as sea spikes, are breaking surface wave crests that produce a specular reflection before they spill because the crest shape is steep and flat. They are the primary scattering mechanism at frequencies higher than L-band. The temporal and Doppler behavior of burst scattering can be seen in Figure 4 (as borrowed from the results of reference [5]) as a function of polarization and wind direction for the aforementioned X-band radar. Burst scattering is strong in amplitude for horizontal polarization, and extremely weak to non-existent for vertical polarization due to multipath. The magnitude of sea spikes is also greater than whitecap or Bragg scattering at L-band and beyond. The phenomenon typically lasts about 0.2 seconds and remains correlated during that time. The Doppler spectrum shows that the speed of sea spikes is faster than that of Bragg resonant waves, and the Doppler spread or bandwidth is narrower than that of Bragg scattering. Unless the waves are breaking towards the radar line of sight, the phenomenon is not visible. Hence no burst scattering is shown for the downwind direction. Reference [2] indicates that cross polarization amplitudes are small for burst scattering, and that the magnitude is equal for all circular polarization channels because of multipath. These effects are shown in Figure 5 from reference [2] for an X-band radar.

3.1.3. Whitecap Scattering

Whitecaps are foamy, rough, surface wave crests that produce noisy scattering reflections from the toppling of the breaking wave crest down the wave front slope. Burst and whitecap scattering tend to occur in sequence, since they both deal with breaking waves. Whitecaps only occur if there is a burst, but bursts can occur without whitecaps. The temporal and Doppler behavior of whitecap scattering can be seen in Figure 6 (as borrowed from the results of reference [5]) as a function of polarization and wind direction for the aforementioned X-band radar. Whitecap scattering amplitudes are similar for vertical and horizontal polarizations and their magnitude is much greater than Bragg scattering when the grazing angles are low or high. The phenomenon lasts seconds in duration, but decorrelates within milliseconds. The Doppler spectrum is very broad and centered proportionately about the phase speed of gravity waves, which is much higher than the Bragg Doppler frequency shift. The upwind data in Figure 6 contains a slight shape difference in the Doppler spectrum between the two polarizations, which should look nearly identical irrespective of polarization such as in the downwind case. Reference [2] states that the difference in vertical and horizontal polarization shift in the upwind direction is due to multipath from direct and reflected paths where constructive interference for the horizontal polarization occurs higher on the wave crest than the vertical direction. The Doppler shift is asymmetric depending on wind direction, with a much higher shift occurring upwind than downwind because of the breaking of the wave [5]. Reference [2] indicates that cross polarization amplitudes are small (by at least 10dB less than the co-polarizations) but follow the co-polarization amplitudes in shape for whitecap scattering. The magnitude is equal for all circular polarization channels because the vertical and horizontal polarizations are not correlated. These effects are shown in Figure 7 from reference [2] for an X-band radar. From examination of Figures 3, 5, and 7, we note that new radar designs may benefit from using cross-polarization responses to minimize sea clutter Bragg, burst, and whitecap scattering in Doppler space.

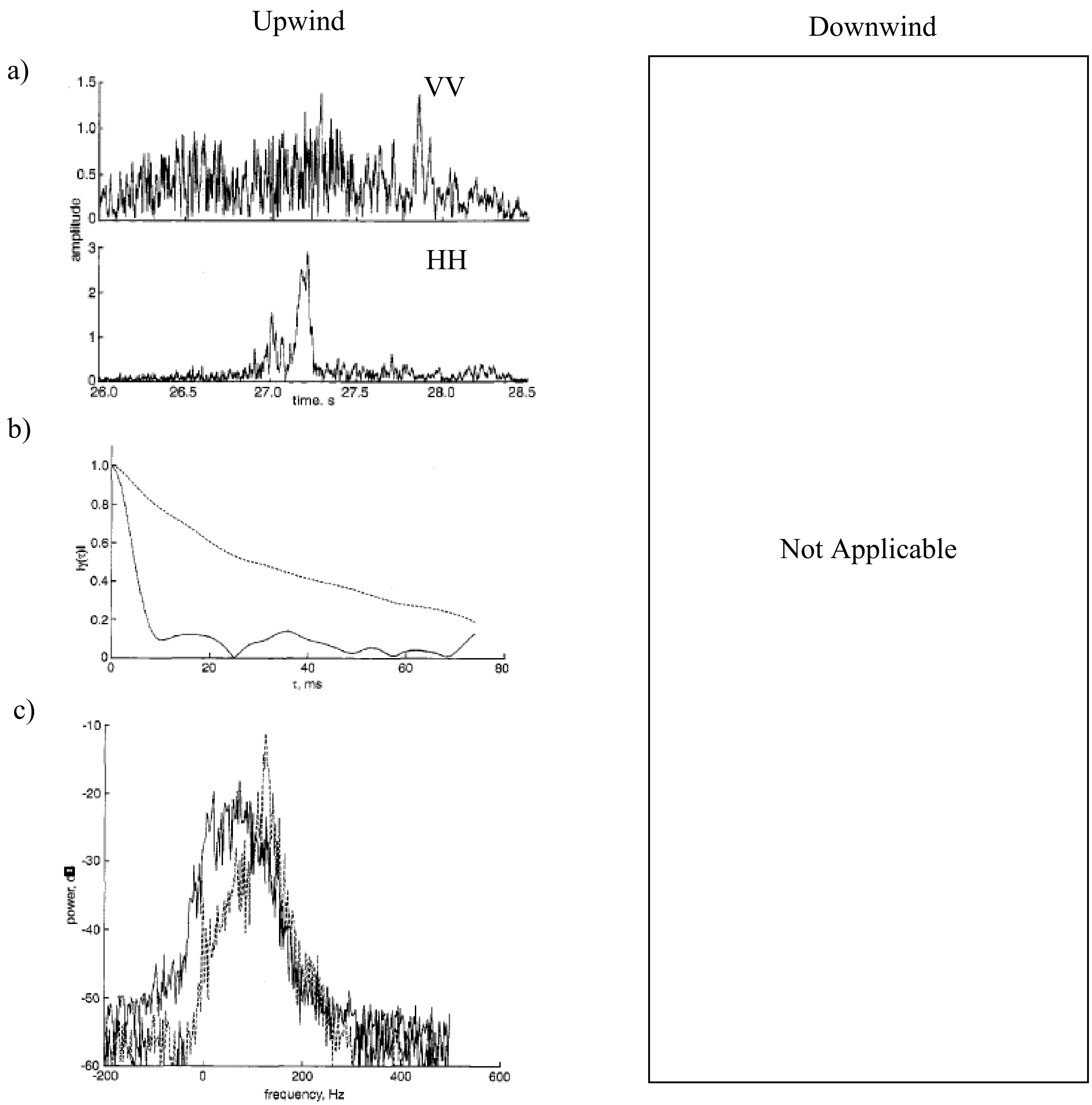

Figure 4. Burst scattering behavior from Ref. [5]
a) Time profile, b) Autocorrelation, c) Doppler spectrum (VV = solid, HH = dotted, unless otherwise specified)

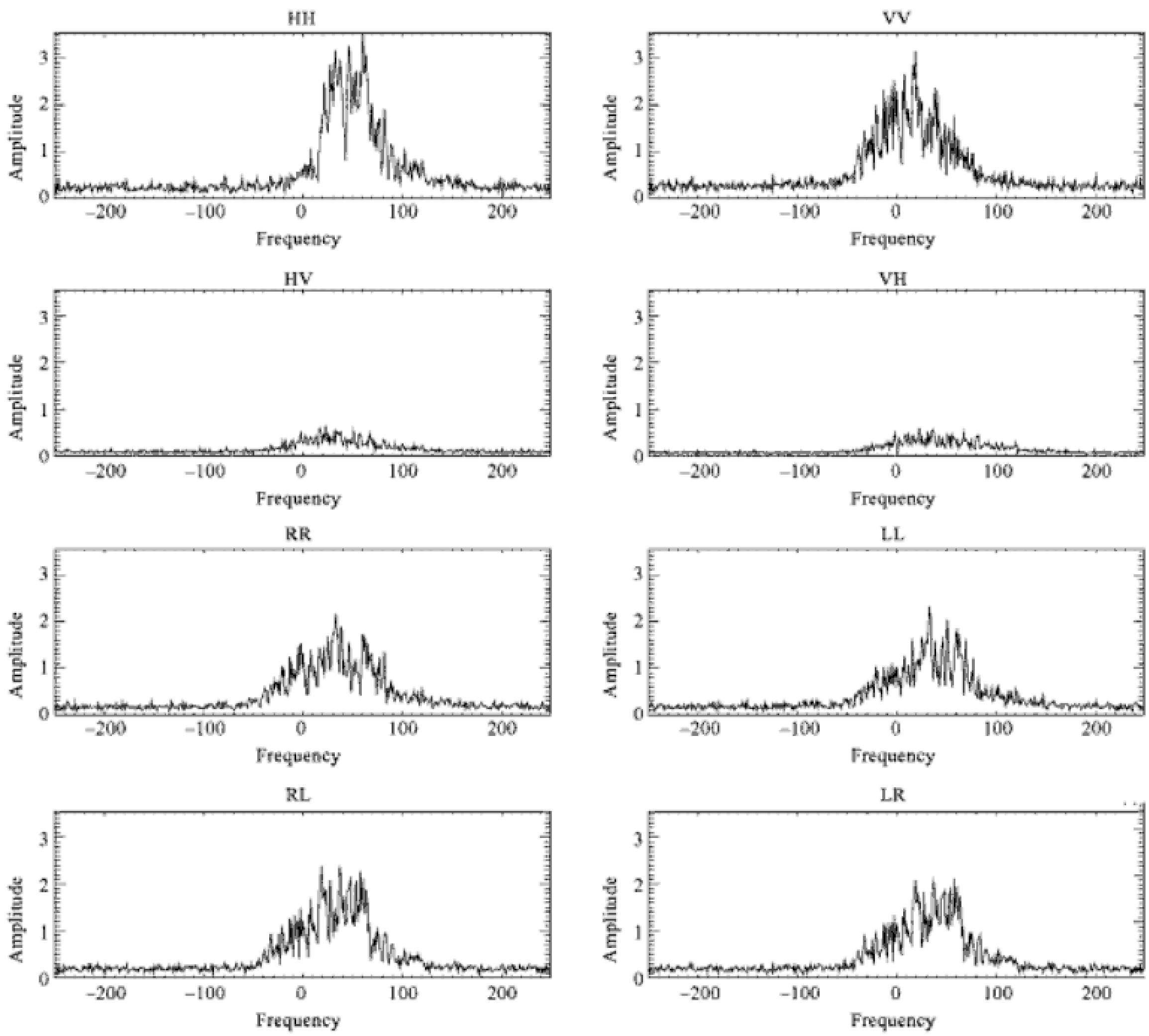

Figure 5. Burst scattering cross-polarization and circular polarization Doppler spectrums at X-band from Ref. [2]

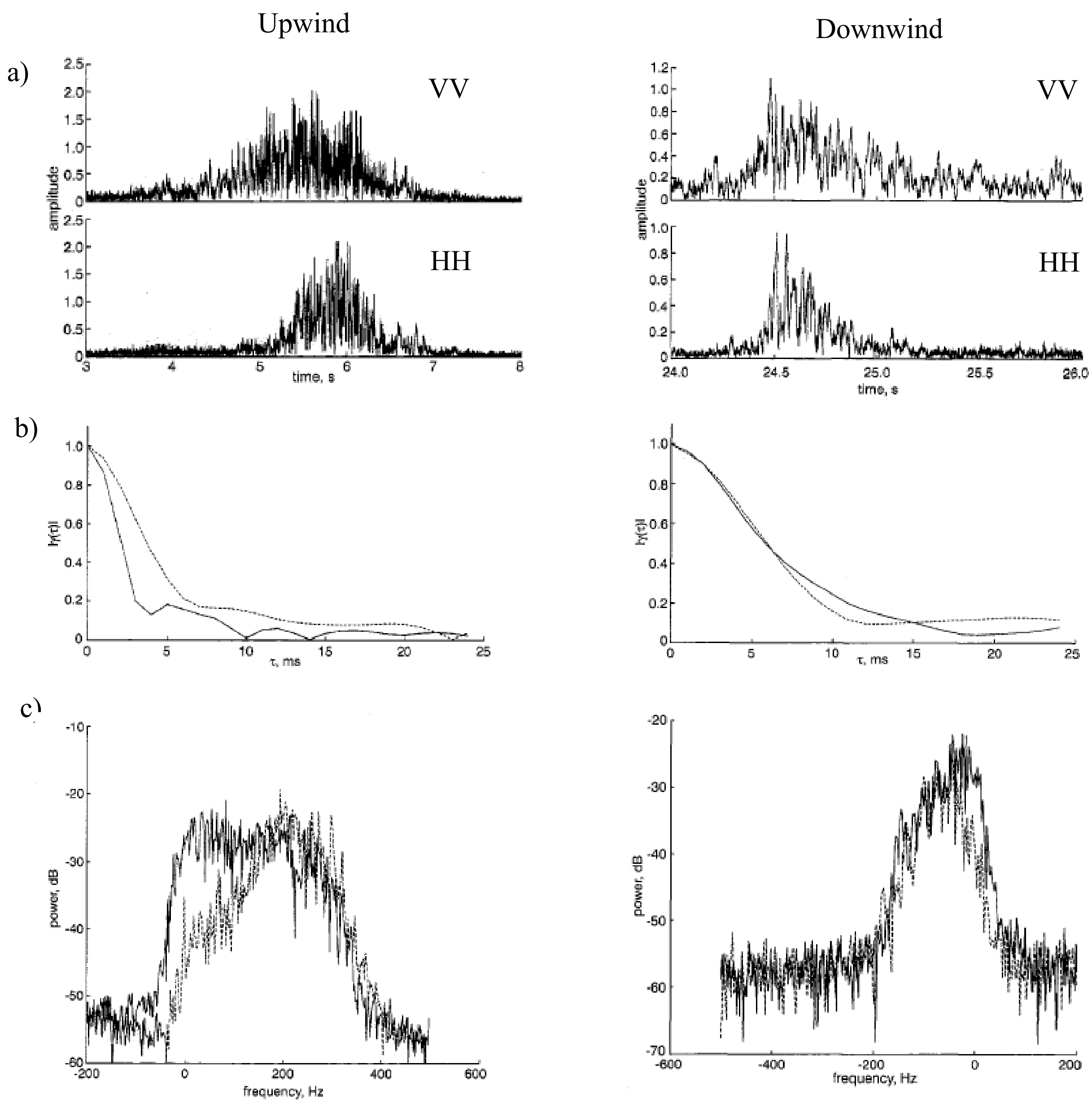

Figure 6. Whitecap scattering behavior from Ref. [5]
a) Time profile, b) Autocorrelation, c) Doppler spectrum (VV = solid, HH = dotted, unless otherwise specified)

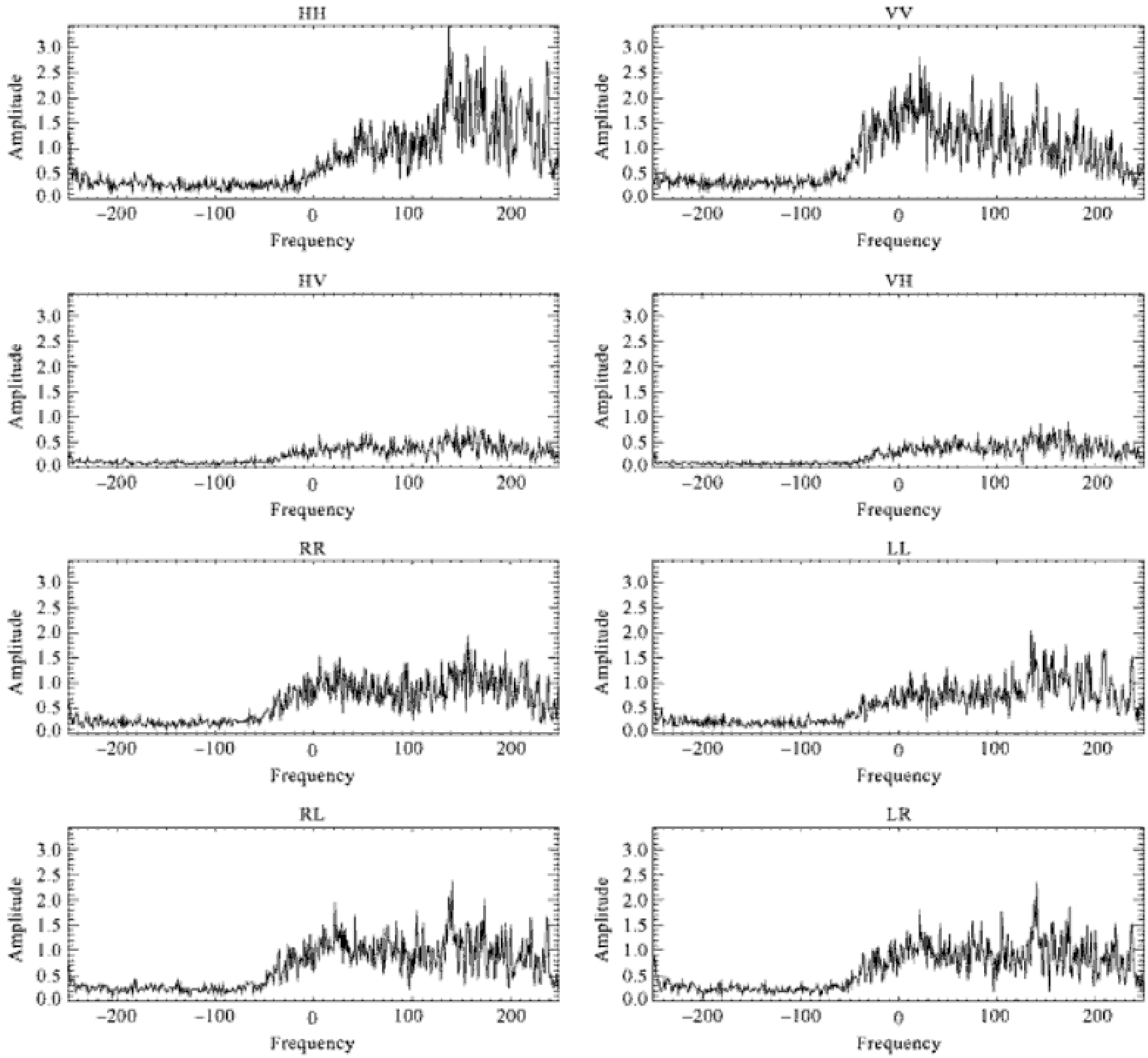

Figure 7. Whitecap scattering cross-polarization and circular polarization Doppler spectrums at X-band from Ref. [2]

3.2. Empirical Doppler Spectrum Shape and Shift

In Figures 2-7, we observe isolated time history instances of Bragg, burst, and whitecap scattering. In general the three components are combined in a single sea clutter Doppler spectrum. The dependencies of the overall spectrum on sea or radar parameters is addressed next.

3.2.1. Low Grazing Angles

For low grazing angles (<10 degrees), the following observations hold. The dependence of the Doppler spectrum on arbitrary wind directions is shown in Figure 8 (as taken from reference [8]) for an X-band radar. A cosinusoidal dependence can be observed for the mean Doppler shift as a function of azimuth angle as the radar line of sight spans from the upwind to downwind directions. Horizontal polarization has a higher shift overall as compared to vertical polarization. Both polarizations reach zero Doppler shift when looking cross-wind. The Doppler spectrum bandwidth tends to be relatively constant, irrespective of azimuth angle [8]. The 3dB-width of the velocity spectrum is approximately the same for both polarizations and corresponds to the upwind orbital velocity empirical formula

$$\mathrm{v_w} \sim 0.24\,U,$$

where U is the wind speed in m/s [9]. The coefficient of U in the formula is an average of typical coefficients for vertical polarization at about 0.15 and horizontal polarization of up to 0.3. Likewise the empirical formula for Doppler shift velocity of the spectrum at X-band in the upwind direction is:

$$\mathrm{v_{Doppler\ \_VV}} \sim 0.25 + 0.18\,U \;\text{ or }\; \mathrm{v_{Doppler\ \_HH}} \sim 0.25 + 0.2\,U.$$

The Doppler spectrum 3dB width and frequency shift can easily be found by $w_{\mathrm{Doppler}} = \frac{2\mathrm{v_w}}{\lambda_{\mathrm{radar}}}$ and $f_{\mathrm{Doppler}} = \frac{2\mathrm{v_{Doppler}}}{\lambda_{\mathrm{radar}}}$, respectively. In addition, the shape and Doppler shift of the spectrum is virtually independent of the radar frequency or the grazing angle. Although these equations are meant for low grazing angles, an example in the next section shows their potential use at higher angles. Bistatic measurements with a small angle of separation between the transmitter and receiver have been taken with no distinction in dependencies versus the monostatic case [10].

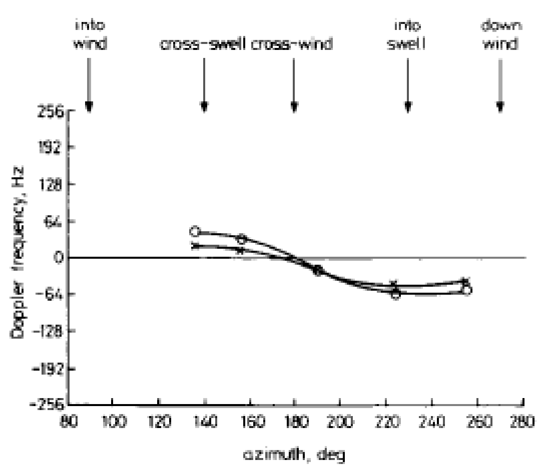

Figure 8. Doppler dependence on azimuth angle at X-band from Ref.[8] (VV=X, HH=O)

3.2.2. High Grazing Angles

In order to examine the Doppler spectrum at higher grazing angles, airborne systems are typically used, since land-based systems tend to be limited to shallow grazing angles. For grazing angles above 10 degrees, the following observations hold. The bandwidth of the Doppler spectrum tends to minimally decrease with increasing frequency and grazing angle [9]. According to reference [9], which did a study at X-band (10.1GHz center frequency with 200MHz bandwidth) at 30-degree grazing, sea clutter is still composed of all three scattering components. However at middle grazing angles (from about 20 to 70 degrees), Bragg scattering is much stronger than whitecap and burst scattering. Burst scattering occurs mainly in the upwind direction, but also randomly at several azimuth angles that are not upwind. Bragg and whitecap amplitudes are similar, but the whitecap scattering time is more spread-out for horizontal polarization. For vertical polarization, the Bragg scattering is much stronger with a smaller temporal spread. This results in decorrelation times for horizontal polarization being slightly less than that of the vertical polarization (by ~2ms). Furthermore, the decorrelation time changes slightly for horizontal and vertical polarizations as a function of azimuth. All other observations of the Doppler spectrum tend to be similar in behavior to the low grazing angle case. For example, Figure 9 shows a 0.2 Hz spectrum of sea clutter at X-band with a 35 degree grazing angle and vertical polarization from reference [9]. The wind speed was 8 m/s (or about 15.6 knots). The wavelength at X-band is approximately 0.03 m. We therefore expect our Doppler spectrum bandwidth and shift from the discussion in section 3.2.1 to be:

$$w_{\mathrm{Doppler\ \_VV}} = \frac{2(0.15)\,U}{\lambda_{\mathrm{radar}}} \approx 80 \text{ Hz, and}$$

$$f_{\mathrm{Doppler\ \_VV}} = \frac{2[0.25+0.18\,U]}{\lambda_{\mathrm{radar}}} \approx 113 \text{ Hz,}$$

which can be verified in the figure where the actual Doppler shift is supposedly -116Hz. Note that the large Doppler shift at about 10 seconds in the spectrum is due to a breaking wave. Likewise, we expect a Ku-band radar at a wavelength of about 18mm with vertical polarization to have spectrum characteristics when interrogating the ocean upwind with a 15 knot wind speed of: $w_{\mathrm{Doppler\ \_VV}} \approx 129$ Hz and $f_{\mathrm{Doppler\ \_VV}} \approx 182$ Hz.

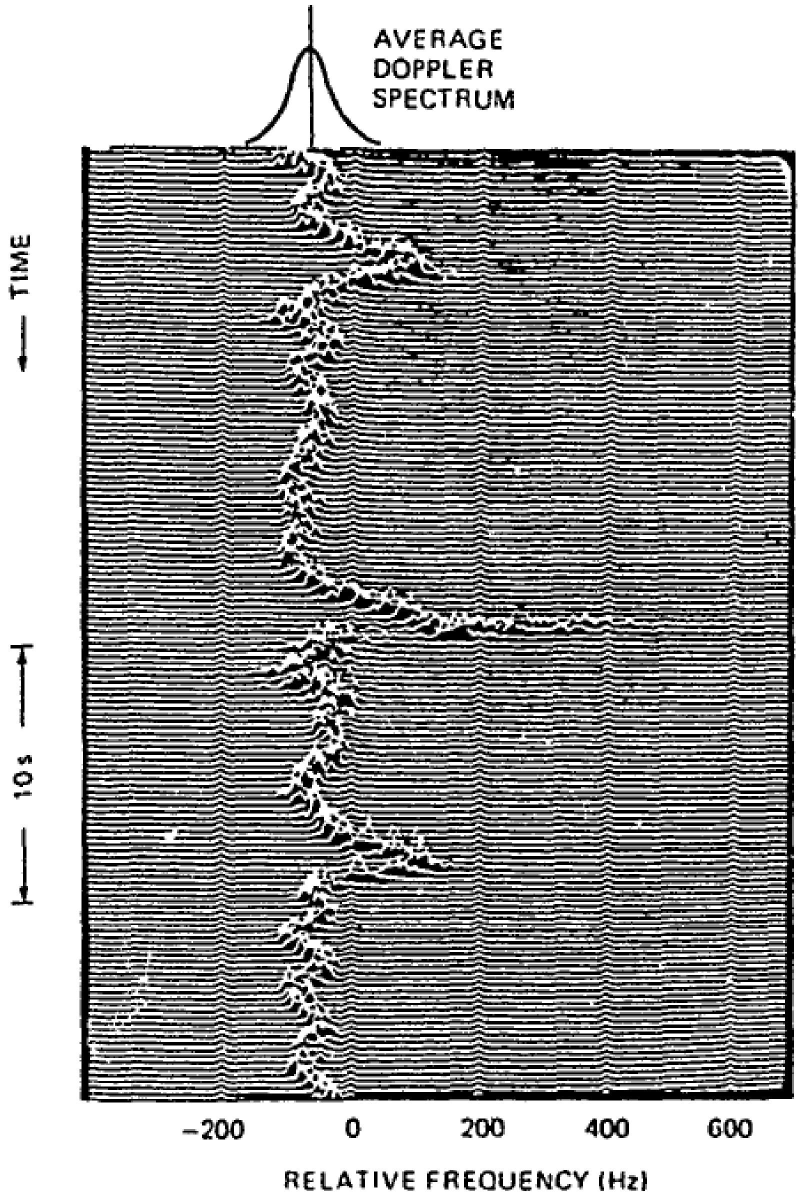

Figure 9. Doppler spectrum at X-band and 35 degree grazing angle from Ref.[9]

4. MATHEMATICAL MODELING OF THE MEASURED DOPPLER SPECTRUM

Section 3 described empirical observations regarding the Doppler spectrum of sea clutter. How to model the Doppler sea clutter shape and shift from a measured Doppler spectrum is addressed next. There are three main alternatives for how to model the Doppler spectrum mathematically given by Lee [11], Walker [5, 6], and Ward, et al. [2]. For the purposes of this document, we shall refer to the model by the first author name in order to distinguish the methods.

4.1. Lee Model

The Lee model states that the overall Doppler spectrum can be decomposed into Gaussian or non-Gaussian lineshapes, or basis functions, representing individual spectra of different scattering mechanisms. If the overall Doppler spectrum is formed over a time period of the signal, T, that is greater than that of the modulation of the gravity waves (which is usually several seconds), then the model proposed by Lee is valid [12]. Lee's lineshapes consist of Gaussian, Lorenztian, and Voigtian basis functions that can be summed to form the Doppler spectrum [11]. More specifically, the Gaussian basis function represents scattering mechanisms from a collection of scatterers with Doppler broadening due to a spread in their speeds. The speed variations of scatterers in the mechanism are from long waves such as gravity waves with smaller capillary wave interaction, or in other words the composite surface model for Bragg scattering. The spectrum for this mechanism is represented as:

$$\Psi_{\text{Gauss}}(f) = \frac{1}{w\sqrt{\pi}}\, e^{-\left(\frac{f-f_{\text{Doppler}}}{w}\right)^2},$$

where f_{Doppler} is the Doppler frequency shift for the mechanism, and w is the spectral bandwidth.

The Lorenztian basis function represents scattering mechanisms with Doppler broadening over a finite scatterer lifetime. These limited lifetime scatterers reside at the crest of breaking waves and are representative of burst scattering. These functions contain a damping term for the spectrum, represented as:

$$\Psi_{\text{Lorentz}}(f) = \frac{\Gamma/2\pi^2}{\left[\left(f-f_{\text{Doppler}}\right)^2+(\Gamma/2\pi^2)^2\right]},$$

where Γ is the damping term, such that its inverse gives the lifetime of the scatterer.

The Voigt basis function represents scattering mechanisms with both Gaussian and Lorenztian characteristics. The Voigt function Doppler spectrum is therefore equivalent to a collection of scatterers with a spread in their speeds that also have a finite lifetime. These scatterers seem to represent whitecap scattering or any nonlinear combination of scattering mechanisms with Lorenztian or Gaussian distributions. This function is represented by:

$$\Psi_{\text{Voigt}}(a,u) = \frac{a}{\pi}\int_{-\infty}^{\infty} \frac{e^{-y^2}}{(u-y)^2+a^2}\,dy,$$

where $u = \left(\frac{f-f_{\text{Doppler\_Voigt}}}{w}\right)$ and $y = \left(\frac{f-f_{\text{Doppler\_Gauss}}}{w}\right)$ are the normalized frequencies for the Voigtian and Gaussian, and $a = \Gamma/2\pi w$ is a ratio of the Lorentzian full-width half maximum lifetime to the full-width increase of the Gaussian by e. In the limit as a tends to zero or infinity, the Voigt basis function becomes purely Gaussian or Lorenztian. From a physical understanding of wave scattering, the decomposition of the Doppler spectrum into the three basis functions is useful. Mathematically, however, one could argue that only Voigt basis functions are required to represent all types of scattering mechanisms. Lee uses the Levenberg-Marquardt algorithm to perform optimized, nonlinear least squares curve fitting of the unknown parameters of the basis functions to a data set.

4.2. Walker Model

The Walker model is a simplified approximation of the Lee model that assumes the overall Doppler spectrum is a sum of only Gaussian lineshapes representing scattering mechanisms from the three-component model. If the overall Doppler spectrum is formed over a time period of the signal, T, that is greater than that of the modulation of the gravity waves (which is usually several seconds), then the model proposed by Walker is valid [12]. Similar to Lee's model the basis function of the Doppler spectra for this model is of the form [5, 6]:

$$\Psi(f) = A\, e^{-\left(\frac{f - f_{\text{Doppler}}}{w}\right)^2},$$

where A is the power spectrum amplitude, f_{Doppler} is the Doppler frequency shift, and w is the spectral bandwidth, all for a particular scattering mechanism. Both the vertical and horizontal polarization spectra are sums of this quantity for different mechanisms of the three-component model, in accordance with the observations made in Figures 2 through 6. That is,

$$\Psi_{\text{VV}} = \Psi_{\text{Bragg\_VV}} + \Psi_{\text{Whitecap}},$$

$$\Psi_{\text{HH}} = \Psi_{\text{Bragg\_HH}} + \Psi_{\text{Whitecap}} + \Psi_{\text{Burst}},$$

where $f_{\text{Doppler}} = \sqrt{\frac{g}{\pi \lambda_{\text{radar}}}}$ for the whitecap and burst mechanisms as given by the gravity wave alone and $f_{\text{Doppler}} = \frac{2}{\lambda_{\text{radar}}}(v_B + v_D)$ for the Bragg mechanism as given by the gravity and capillary wave interactions mentioned previously in the composite-surface Bragg model. The power spectrum amplitude for the Bragg Gaussian shape is distinct for the different polarizations, which is not the case for whitecap scattering. Burst scattering does not exist for vertical polarizations, hence its absence from that model. The spectral bandwidth of Bragg and whitecap scattering is consistent across polarization models for the respective components. Walker gives formulas for the Bragg RCS values in [6]. However, in general optimization techniques such as Levenberg-Marquardt are used to find the best fit to the real data while estimating the spectral width, Doppler shift, and power spectrum amplitude parameters [7].

Table 2 and Figure 10 show sample Doppler spectra and Walker model fit parameters, respectively, at Ku-band and a 6 degree grazing angle. Figure 10a) results are for a wave tank experiment with 10 m/s wind speeds; Figure 10b) results are for 2.3 m breaking waves (i.e. no Bragg scattering). Amplitude results for the mechanisms are normalized to the Bragg scattering vertical polarization value. Note the expected larger Doppler shift, wider spectrum widths, and larger whitecap and burst amplitudes for the breaking wave scenario.

Table 2. Walker model parameters at 15.75GHz and 6 degree grazing angle from Ref [6]

Wind Speed (m/s)	$\frac{A_{Bragg\_HH}}{A_{Bragg\_VV}}$ (dB)	$\frac{A_{whitecap}}{A_{Bragg\_VV}}$ (dB)	$\frac{A_{Burst}}{A_{Bragg\_VV}}$ (dB)	w_{Bragg} (Hz)	$w_{whitecap}$ (Hz)	w_{Burst} (Hz)
10	-20.74	-6.17	-4.89	27.3	23.2	30.1
2.3m Breakers	-25	10.2	22.5	57	59.5	50

a)
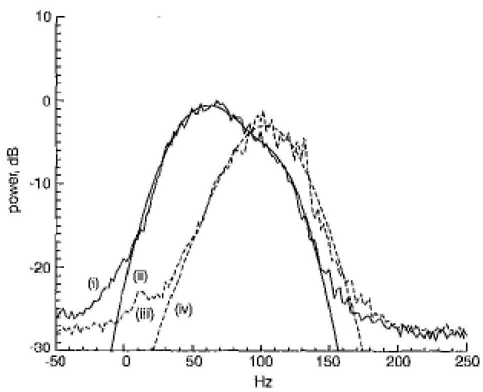

b)
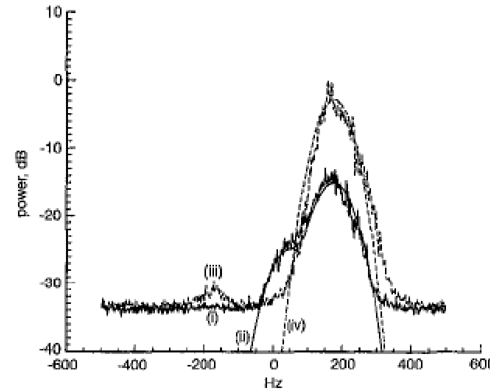

Figure 10. Walker model Ku-band Doppler spectra at 6 degree grazing angle from Ref [6] i)=VV data, ii)=VV model, iii)=HH data, iv)=HH model a) 15.75GHz with 10m/s wind speed and b) 15.75GHz with 2.3 m breaking waves

4.3. Ward, et al. Model

The Ward, et al. model assumes that the Doppler spectrum shape must be modeled by a random process. If the Doppler spectrum is formed over a time period of the signal, T, that is less than that of the modulation of gravity waves but longer than the decorrelation time of burst and whitecap scattering (which is usually a tenth of a second), then the Ward model is appropriate [12]. The Ward, et al. model is effectively a short-time Doppler spectrum that will vary temporally over the gravity wave modulation duration [2] as shown in Figure 11 a) from reference [8]. Ward, et al. consider this power spectrum as gamma variate in keeping with the compound K-distribution models that have proven useful for sea clutter amplitude characterization. The model authors point out that the sea clutter spectra is non-Gaussian as shown in Figures 11b) and c) for the normalized second order moments of the Doppler spectrum, for both vertical and horizontal polarizations, respectively. The Doppler spectrum basis function for this model is of the form:

$$\Psi(2\pi f) = x\widehat{\Psi}(2\pi f), \text{ for}$$

$$\widehat{\Psi}(2\pi f) = \frac{e^{-\left(\frac{[2\pi(f-f_{\text{Doppler}}]}{2w^2}\right)^2}}{\sqrt{2\pi w^2}},$$

where x is the gamma variate local power that does not fluctuate over the short-time power spectrum computation and $\widehat{\Psi}(2\pi f)$ is a Gaussian lineshape of the Walker model. The Ward, et al. model gives an effective shape parameter that depends on the normalized second order moments of the Doppler spectrum:

$$\frac{1}{v_{eff}} = \frac{\langle \Psi(2\pi f)^2 \rangle}{\langle \Psi(2\pi f) \rangle^2} - 1,$$

where $\langle\,\rangle$ denotes expectation. This simple model can be augmented to include mean Doppler shift and width variations for resonant and non-resonant wave scattering phenomenology as a sum of Gaussian components much like the Walker model. The Doppler spectrum in this case would become:

$$\Psi(2\pi f) = x \frac{A\hat{\Psi}(2\pi f, w_{Bragg}, 0) + x\hat{\Psi}(2\pi f, w_{Breaking}, 2\pi f_{\mathrm{Doppler}})}{A+x},$$

where $\hat{\Psi}(2\pi f)$ is as above, w_{Bragg} and $w_{Breaking}$ represent the spectral widths of the Bragg and breaking wave phenomena, and f_{Doppler} is the breaking wave Doppler shift since Bragg scattering tends to have near zero Doppler shift.

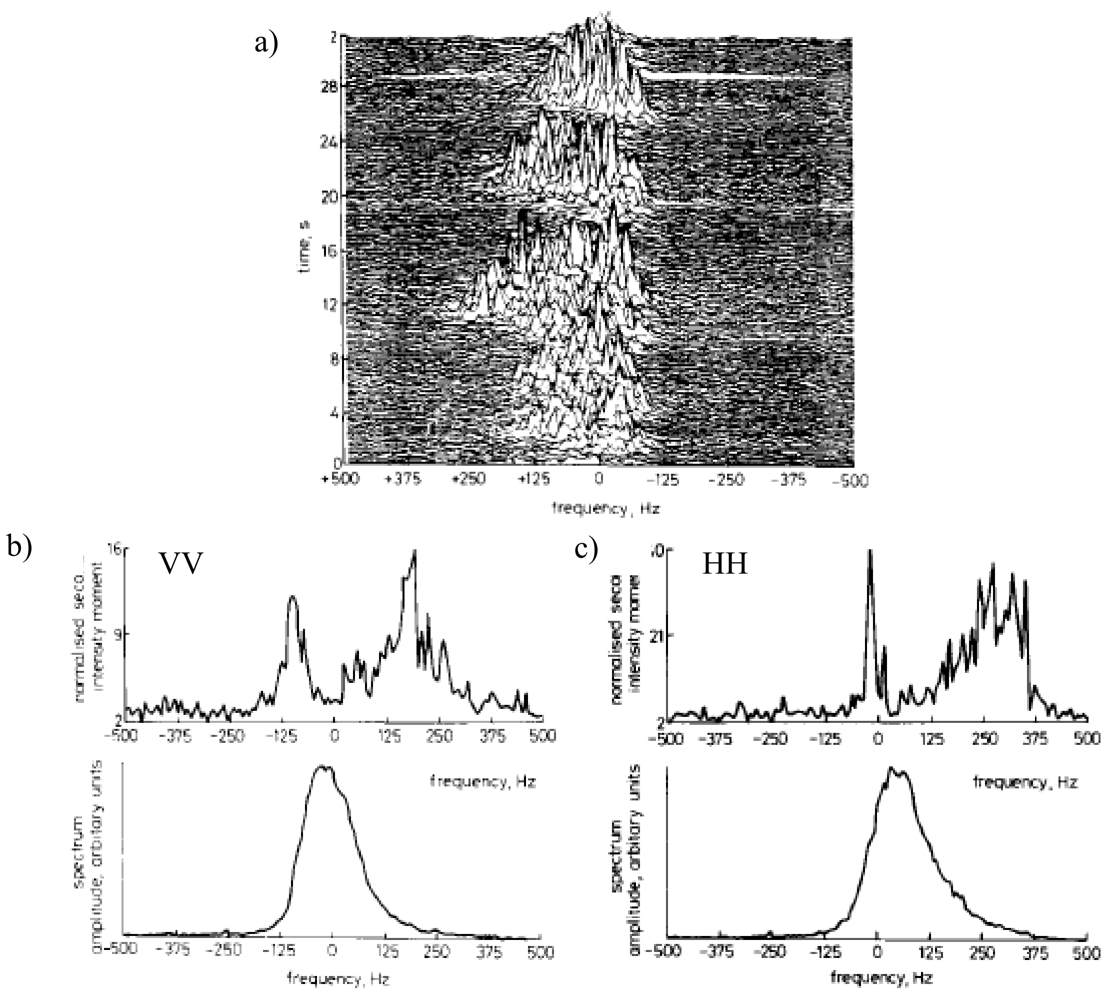

Figure 11. Short-time Doppler spectrum characteristics of a range cell from Ref.[8] a) Short-time Doppler spectrum, b) Vertical polarization second order moments and Doppler time-averaged spectrum, c) Horizontal polarization second order moments and Doppler time-averaged spectrum

5. ELECTROMAGNETIC SCATTERING PREDICTION OF SEA CLUTTER

Electromagnetic scattering prediction of sea clutter involves approximating the rough surface characteristics of the sea as many conducting flat plates, known as facets, with different tilt angles [2] to mimic the behavior of surface waves. Hydrodynamic models from oceanography are incorporated into the electromagnetic scattering prediction process. No single model exists to completely describe the wave structure of the sea surface or electromagnetic scattering at all grazing angles. The more widely used formulations are given in the following subsections. The majority of the literature focuses on approximations for the RCS of sea clutter and not the complex scattered electric field from which a Doppler spectrum could be computed. While at first glance it may appear that this section seems out of place with respect to the discussion on sea clutter Doppler characteristics, we nevertheless provide it here as a complement to the foregoing discussion.

5.1. Hydrodynamic Models

Electromagnetic scattering models often use empirical models from oceanography as an input for how wave energy is distributed across space and temporal frequency, which is otherwise known as a wave spectra. According to empirical linear modeling results, sea surface height and slope are approximately a Gaussian process. Hydrodynamic models that give an average power spectrum for this Gaussian process are the Pierson-Moskowitz and Elfouhaily models. The Pierson-Moskowitz model below is only useful for gravity waves greater than 5 cm:

$$S_\eta(q,\omega) = \frac{b}{4\pi} q^{-4} e^{-0.6\left(\frac{g}{qU_{10}^2}\right)^2} \cos^{2\mathrm{n}}\left(\frac{\theta_\omega}{2}\right) \frac{(2n!!)}{(2n-1)!!} \delta\left(\omega - \sqrt{gq}\right),$$

where q is the magnitude of the spatial frequency, ω is the temporal frequency, b is the Phillips equilibrium parameter for the sea, g is the acceleration due to gravity, U_{10} is the wind speed 10 m above the sea surface, θ_ω is the angle between the spatial frequency and wind vector direction, n is an angular spreading parameter such that $2n!! = 2n(2n-2)(2n-4) \ldots 2$ and $(2n-1)!! = (2n-1)(2n-3) \ldots 1$. The Elfouhaily model is much more complicated and is meant to incorporate capillary wave motion. The reader is referred to [2] for the equations comprising this model if they are of interest. Further, more complicated models exist to encompass breaking wave phenomenology.

5.2. Electromagnetic Models

As with all electromagnetic scattering predictions, the full numerical solution to the scattering problem involves solving a complicated electric field integral equation derived from Maxwell's equations. In the case of the scattered field from the sea surface, the coupled magnetic and electric field integral equations are known as the Stratton-Chu equations [2]. Several simplified approaches to solving these equations exist with applicable constraints.

5.2.1. High Grazing Angles

At high grazing angles from about 60 to 90 degrees, a perfect conductor and physical optics approximation can be used to find the RCS of sea clutter as below:

$$\sigma^0 = \frac{k^4}{k_z^2}\frac{1}{\pi}\int e^{-2j\vec{k}_H\cdot\vec{v}}e^{-4k_z^2\langle\eta^2\rangle(1-\rho(\vec{v}))}\,d^2x,$$

where k is the wave number, $\vec{k}_H$ is the wave vector horizontal component, k_z is the wave vector component in the z-direction, $\langle\eta^2\rangle$ is the expectation of the square of the wave height, and $\rho(\vec{v})$ is the normalized autocorrelation function of the surface height fluctuations as a function of the component in the xy-plane of the position vector $\vec{x}$. A further approximation can be made strictly for Bragg scattering of $\sigma^0 = 8\pi k^4[S_\eta(-2\vec{k}_H) + S_\eta(2\vec{k}_H)]$.

5.2.2. Mid Grazing Angles

At all other grazing angles, sea clutter has a polarization dependence such that the perfect electric conductor and physical optics model is not valid. At mid-grazing angles from about 15 to 60 degrees, the RCS of resonant waves is dominant and a composite model is used. This model breaks up the wave spectrum into long and short waves, or in other words gravity and capillary waves, according to a cutoff frequency. That cutoff is a few times larger than the resonant wave number of $\vec{k}_{res} = 2(\vec{k}_H + k_z\nabla\eta_L)$, where $\nabla\eta_L$ is the slope of the long waves. The RCS for mid-grazing angles is the given by:

$$\sigma_{Pol}^0 = \int P(\nabla\eta_L)\,\sigma_{Pol}^0(\nabla\eta_L)d^2\nabla\,\eta_L,$$

where Pol is the polarization VV, HH, or VH; $\sigma_{Pol}^0(\nabla\eta_L)$ is the normalized backscatter RCS from the short wave ripples atop the long wave slope; and $P(\nabla\eta_L)$ is the joint probability density function of the correlation of the long wave surface slope to the surface height of the wave spectrum. The reader is referred to [2] for the intricate equations of these variables.

5.2.3. Low Grazing Angles

The composite model fails to account for multipath propagation, shadowing, and breaking wave backscatter at low grazing angles. The physical optics approximation is likewise inapplicable to this scenario. The sea surface can be modeled as a corrugated surface for these angles. The RCS is then:

$$\sigma^0 = \frac{1}{4kL}\left|\int_{-L/2}^{L/2}\left[(q(y) + q_{ap}(y))e^{-2ik_z\,\eta(y)} - 2k_z\right]e^{-2ik_H y}\,dy\right|^2,$$

where $q(y)$ is the corrugated surface field contribution at y, $q_{ap}(y)$ is the scattered field contribution from the field of adjacent corrugated planes induced by the field at y, and L is the length of the patch of corrugated sea.

5.3. Empirical RCS Models

Electromagnetic prediction of sea clutter RCS is far from simple and computationally fast. Empirical models are a viable alternative to physical modeling. Two models developed in the 1970's that have been in use are: the Royal Radar Establishment model and the Georgia Institute of Technology model.

5.3.1. Royal Radar Establishment (RRE) Model

The Royal Radar Establishment of the United Kingdom proposed an empirical model for grazing angles below 10 degrees for the RCS of sea clutter averaged over all aspect angles at 9-10 GHz that varies with grazing angle, polarization, and sea state. The model, which has been in use for over 30 years, is:

$$\sigma^0 = \mathrm{a}[\mathrm{s}] + \mathrm{b}[\mathrm{s}] \log_{10}\left(\frac{180\psi}{\pi}\right), \text{ for } \psi \leq 1°,$$
$$\sigma^0 = \mathrm{a}[\mathrm{s}] + \mathrm{c}[\mathrm{s}] \log_{10}\left(\frac{180\psi}{\pi}\right), \text{ for } \psi > 1°,$$

where s is the sea state, ψ is the grazing angle, and a, b, c are discrete functions of the sea state (1-6) and polarizations as below:

$$\mathrm{a}_{\mathrm{HH}}[\mathrm{s}] = [-52, -46, -42, -39, -37, -35.5],$$
$$\mathrm{a}_{\mathrm{VV}}[\mathrm{s}] = [-51.5, -45.5, -41, -38.5, -36, -34.5],$$

$$\mathrm{b}_{\mathrm{HH}}[\mathrm{s}] = [21, 17.5, 12.5, 10.5, 7, 3.5],$$
$$\mathrm{b}_{\mathrm{VV}}[\mathrm{s}] = [15, 12, 11.5, 11, 9.5, 8],$$

$$\mathrm{c}_{\mathrm{HH}}[\mathrm{s}] = [1.015, 3.39, 2.03, 1.35, 2.03, 2.37],$$
$$\mathrm{c}_{\mathrm{VV}}[\mathrm{s}] = [8.2, 9.5, 8, 7.5, 7, 6.5].$$

5.3.2. The Georgia Institute of Technology (GIT) Model

The Georgia Institute of Technology developed a model for the RCS of sea clutter that is dependent on sea state, grazing angle, and radar wavelength for frequencies from 1-100 GHz. For frequencies from 1-10 GHz, the model assumes a wind velocity of

$$U = 3.16s^{0.8},$$

with an average wave height of

$$h_{avg} = 0.00452U^{2.5},$$

and a roughness parameter

$$\sigma_\phi = (14.4\lambda_{radar} + 5.5)\frac{\psi h_{avg}}{\lambda}.$$

The model uses parameters for multipath interference, wind direction dependence, and sea state variation of

$$A_i = \frac{\sigma_\phi^4}{1+\sigma_\phi^4},$$
$$A_u = e^{0.2\cos(\theta_w)(1-2.8\psi)(\lambda+0.015)^{-0.4}}, \text{ and}$$
$$A_w = \left(\frac{1.94U}{1+(U/15.4)}\right)^{1.1/(\lambda+0.015)^{0.4}},$$

respectively, where θ_w is the wind direction relative to the radar look angle. The RCS for vertical and horizontal polarization is then:

$$\sigma_{HH}^0 = 65.91 + 10\log_{10}(\lambda\psi^{0.4}A_i A_u A_w), \text{ and}$$
$$\sigma_{VV}^0 = \sigma_{HH}^0 - 1.05\log_e\left(h_{avg} + 0.015\right) + 1.09\log_e\lambda + 1.27\log_e(\psi + 0.0001) + 9.7.$$

Arctic Ocean Ripples from Ref. [13]

6. SUMMARY

In sum, the Doppler spectrum characteristics of sea clutter are mainly attributed to resonant and non-resonant surface wave behavior. The two types of resonant surface waves are capillary and gravity waves, or in other words ripples and long waves. These waves cause Bragg scattering behavior based on experimental observation. Non-resonant, breaking wave behavior causes specular or noisy reflections known as burst and whitecap scattering, respectively. Bragg scattering is further broken down into capillary and gravity wave resonant scattering in the composite surface scattering model. At low radar frequencies (e.g. HF and VHF), Bragg scattering is the dominant mechanism, whereas at higher frequencies (e.g. L-band and above), breaking waves are the primary scattering effects at all but mid-grazing angles. Bragg, burst, and whitecap scattering comprise the three-component scattering model of the Doppler spectrum.

The Doppler characteristics of these individual scattering components have generally been well-studied empirically to understand overall sea clutter Doppler behavior under various parameters including grazing angle, frequency, look angle in relation to wind direction, and polarization, although low grazing angle and low-frequency experiments dominate the literature. Useful rules of thumb at X-band for low grazing angle Doppler spreading and shifting as a function of wind speed are given in Section 3.2.1. No such rules of thumb exist for the higher grazing angles in the literature, yet the equations may possibly still be applicable. Notwithstanding, from empirical results, several mathematical models have been proposed to estimate measured sea clutter Doppler spectra shift, shape, and amplitude. The principal models that appear in the literature are by Lee, Walker, and Ward, et al. The models of Lee and Walker assume that the power spectrum is formed over a period greater than several seconds to encompass all scattering mechanisms, whereas the Ward, et al. model forms a short-time spectrum to look at variations of breaking wave mechanisms as a function of the modulation of gravity wave scattering. The models by Lee and Walker both assume that the overall Doppler spectrum can be decomposed into a sum of simple mathematical formulas that represent individual scattering components. The Ward model assumes a probabilistic formulation more consistent with the models used for sea clutter amplitude characterization. These models might be used to analyze sea clutter Doppler spectrums at higher grazing angles to determine rules of thumb that depend on wind speed or sea state.

"Neither can the wave that has passed by be recalled, nor the hour which has passed return again."

-Ovid

7. REFERENCES

1. M. I. Skolnik, *Introduction to radar systems, 3rd Edition (U)*, McGraw-Hill, Boston, MA (U), 2001.

2. K. D. Ward, R. J. A. Tough, and S. Watts, *Sea clutter: Scattering, the K-distribution, and radar performance (U)*, The Institution of Engineering and Technology, London, UK (U), 2006.

3. Beaufort Sea Scale, http://www.delta-s.org/weer/wind-at-sea.jpg

4. D. D. Crombie, "Doppler spectrum of sea echo at 13.56 Mc/s (U)," *Nature*, vol. 175, pp. 681-682, Apr. 16, 1955.

5. D. Walker, "Doppler modeling of radar sea clutter (U)," *IEE Proc. on Radar, Sonar, and Navigation*, vol. 148, no. 2, pp. 73-80, Apr. 2001.

6. D. Walker, "Experimentally motivated model for low grazing angle radar Doppler spectra of the sea surface *(U)*," *IEE Proc. on Radar, Sonar, and Navigation*, vol. 147, no. 3, pp. 114-120, June 2000.

7. L. Rosenberg and N. J. Stacy, "Analysis of medium grazing angle X-band sea-clutter Doppler spectra (U)," *IEEE*, 2008.

8. K. D. Ward, C. J. Baker, S. Watts, "Maritime surveillance radar part 1: Radar scattering from the ocean surface (U)," *IEE Proceedings*, vol. 137, pt. F, no. 2, Apr. 1990.

9. L.B. Wetzel, "Sea Clutter (U)," *Naval Research Laboratory Report 9244 (U)*, September 28, 1990.

10. V. W. Pidgeon, "Doppler dependence of radar sea return (U)," *Journal of Geophysical Research*, vol. 73, no. 4, pp. 1333-1341, Feb. 1968.

11. P. H. Y. Lee, et al., "Power spectral lineshapes of microwave radiation backscattered from sea surfaces at small grazing angles (U)," *IEE Proc. on Radar, Sonar, and Navigation*, vol. 142, no. 5, pp. 252-258, Oct. 1995.

12. S. Watts, "Radar sea clutter modeling and simulation - Recent progress and future challenges (U)," *The Institution of Engineering and Technology*, UK (U).

13. Arctic Ocean Ripples, http://science.nationalgeographic.com/wallpaper/science/photos/coastlines-gallery/arctic-ocean-ripples/

DISTRIBUTION

1	MS 1330	J. J. Hudgens	5240	
1	MS 1330	B. L. Burns	5340	
1	MS 0519	T. J. Mirabal	5341	
1	MS 0519	S. Gardner	5342	
1	MS 1330	S. D. Bensonhaver	5342	
1	MS 1330	T. P. Bielek	5342	
1	MS 1330	J. D. Bradley	5342	
1	MS 1330	A. W. Doerry	5342	
1	MS 1330	D. W. Harmony	5342	
1	MS 1330	J. A. Hollowell	5342	
1	MS 1330	M. S. Murray	5342	
1	MS 1330	C. Musgrove	5342	
1	MS 1332	R. Riley	5342	
1	MS 1330	J. A. Rohwer	5342	
1	MS 1330	B. G. Rush	5342	
1	MS 1330	G. J. Sander	5342	
1	MS 1330	D. G. Thompson	5342	
1	MS 1330	W. H. Hensley	5344	
1	MS 1330	S. Nance	5344	
1	MS 1330	K. W. Sorensen	5345	
1	MS 0529	B. C. Brock	5345	
1	MS 1330	D. F. Dubbert	5345	
1	MS 0529	G. K. Froehlich	5345	
1	MS 1330	F. E. Heard	5345	
1	MS 1330	G. R. Sloan	5345	
1	MS 1330	S. M. Becker	5348	
1	MS 0503	P. A. Dudley	5348	
1	MS 1330	O. M. Jeromin	5348	
1	MS 1330	D. M. Small	5348	
1	MS 1330	B. L. Tise	5348	
1	MS 0519	D. M. Brouhard	5349	
1	MS 0519	C. Smithpeter	5354	
1	MS 0519	D. L. Bickel	5354	
1	MS 0519	A. Martinez	5354	
1	MS 0519	A. M. Raynal	5354	
1	MS 0519	R. Pai	5354	
1	MS 0899	Technical Library	9536	(electronic copy)
1	John Fanelle	General Atomics ASI, RSG		(electronic copy)

Note: Further distribution to General Atomics employees is authorized.

Sandia National Laboratories